Proceedings of the European Conference "Physics of Magnetism" (PM'08), Poznań 2008

Aharonov–Bohm Effect and Valley Polarization in Nanoscopic Graphene Rings

A. Rycerz[a,b]

[a]Institut für Theoretische Physik, Universität Regensburg

D-93040 Regensburg, Germany

[b]Instytut Fizyki im. Mariana Smoluchowskiego, Uniwersytet Jagielloński*

Reymonta 4, PL-30-059 Kraków, Poland

The conductance of an Aharonov–Bohm interferometer is studied in a tight-binding model of graphene. Two point contacts with zigzag edges, which function as valley filters, are connected by a ring with an irregular boundary. We find that the narrowest rings show strong current suppression and nearly sinusoidal magnetoconductance oscillations, whereas for wide rings higher harmonics are equally represented. In the intermediate width range, oscillations with a basic periodicity are suppressed when two valley filters have opposite polarity, while higher harmonics are unaffected. The effect is interpreted in terms of a relatively weak intervalley scattering in the system.

PACS numbers: 73.23.−b, 73.63.Rt, 85.35.Ds

1. Introduction

The discovery of graphene [1] has led physicists to reexamine classic effects from mesoscopic physics [2], mainly in search are novel features that arise from the unusual conical band structure of a carbon monolayer. However, the Aharonov–Bohm effect [3, 4] has received so far little attention. Preliminary experiments have been reported [5], the energy spectrum of a *closed* graphene ring was also studied theoretically as a function of the enclosed magnetic flux Φ by Recher et al. [6]. Here we study the electron transport through an *open* graphene ring, contacted to reservoirs by ballistic point contacts. Our work builds on an earlier finding [7] that a single-mode point contact with zigzag edges operates as a valley filter. Depending on whether the Fermi level in the point contact lies in the conduction or valence band, the transmitted electrons occupy states in one or the other valley of the band structure.

We find that in a few-mode graphene rings the conductance is strongly suppressed for any polarity of the valley filters with small, nearly sinusoidal magnetoconductance oscillations, which show the expected $\Delta\Phi = h/e$ periodicity. Instead, in a multimode ring the conductance oscillates between 0 and the maximal quantum value $2e^2/h$ (limited by valley-filtering point contacts) with higher harmonics equally represented in a Fourier spectrum. In the intermediate range, however, the lowest harmonic dominates the spectrum only if the two filters have the same polarity. For opposite polarity a *period doubling* appears: The lowest harmonic is suppressed while the second and higher harmonics are unaffected or enhanced. We attribute the period doubling to a relatively long intervalley scattering time, which causes that the electron have to travel more than once along the ring to flip the valley pseudospin.

2. Aharonov–Bohm interferometer in graphene

The analysis starts from the tight-binding model of graphene, with Hamiltonian

$$H = \sum_{i,j} \tau_{ij} |i\rangle\langle j| + \sum_i V_i |i\rangle\langle i|. \tag{1}$$

The system is coupled to the vector potential $\boldsymbol{A}$ through the hopping matrix element

$$\tau_{ij} = -\tau \exp\left(\frac{2\pi \mathrm{i}}{\Phi_0} \int_{\boldsymbol{R}_i}^{\boldsymbol{R}_j} \mathrm{d}\boldsymbol{r} \cdot \boldsymbol{A}\right), \tag{2}$$

with $\tau = 2.7$ eV the hopping energy and $\Phi_0 = h/e$ the flux quantum. The orbitals $|i\rangle$ and $|j\rangle$ are nearest neighbors on a honeycomb lattice (with lattice points $\boldsymbol{R}_i$), otherwise $\tau_{ij} = 0$. The energy-independent Fermi velocity v_F near the Dirac point equals $v_\mathrm{F} = \frac{1}{2}\sqrt{3}\tau a/\hbar \approx 10^6$ m/s, with the lattice constant $a = 0.246$ nm. The electrostatic potential $V_i = V(x_i)$ varies only along the axis connecting the input and output point contacts (see Fig. 1). Namely, the potential equals U at the first constriction ($0 < x < l$, where l is the constriction length), U' at the second constriction ($l + L_\mathrm{C} < x < 2l + L_\mathrm{C}$, with $L_\mathrm{C} = \sqrt{4R^2 - w^2}$, where R is the ring radius and w is the constriction width), and zero everywhere else. By varying U and U' at a fixed Fermi energy μ_∞ in the external leads, we can vary the Fermi energies $\mu = \mu_\infty - U$ and

* Permanent address.

$\mu' = \mu_\infty - U'$ in the two constrictions. We took $\mu_\infty = \tau/3$ to work with heavily doped graphene leads, while remaining at sufficiently small Fermi energy that the linearity of the dispersion relation holds reasonably well. The constriction parameters $w = 10\sqrt{3}a$ and $l = 16a$ are chosen to provide valley polarizations above 90% [7].

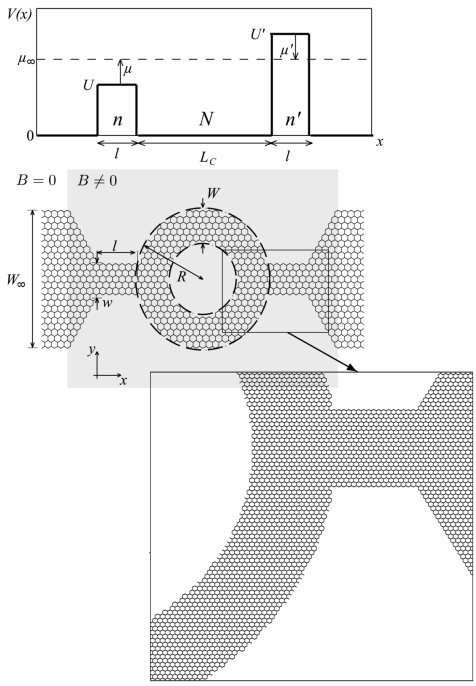

Fig. 1. Graphene ring with an approximately circular boundary attached to graphene leads (middle part) and corresponding potential profile (above). Constrictions with zigzag edges between leads and the ring allows one to control input and output valley polarizations by varying the electrostatic potentials U and U'. A magnified section (bottom part) of the ring with $R = 35\sqrt{3}a$ and $W = 10\sqrt{3}a$ used in our simulations, which shows the irregularity of the boundary.

We denote the number of transmitted modes through the first constriction by n and through the second constriction by n'. A positive number indicates that the Fermi level lies in the conduction band, while a negative number indicates that the Fermi level lies in the valence band. For example, as shown in Ref. [7], the case $-3\Delta/2 < \mu' < 0 < \mu < 3\Delta/2$ (with $\Delta = \pi\hbar v/w$) corresponds to $n = 1$, $n' = -1$ (valley filters of opposite polarity), while the case $0 < \mu, \mu' < 3\Delta/2$ corresponds to $n = n' = 1$ (valley filters of the same polarity). The interferometer is modeled by a ring with an irregular, approximately circular boundary, constructed by keeping only the lattice sites within an annulus formed by two concentric circles. Because the boundaries are not uniform, the number of modes that can propagate along the ring is not well defined. We label the data by the number of modes N in zigzag-edge nanoribbon of width W, short sections of which are still present in the ring. To vary N, we keep the radius fixed at $R = 35\sqrt{3}a$ and vary the inner radius. Ring widths $W/\sqrt{3}a = 5 \div 20$ correspond to $N = 1 \div 7$.

We take the vector potential $\boldsymbol{A} = (A_x, 0, 0)$ with

$$A_x = \begin{cases} By, & -\frac{W_\infty - w}{\sqrt{3}} < x < 2l + L_C + \frac{W_\infty - w}{\sqrt{3}}, \\ 0, & \text{otherwise.} \end{cases} \quad (3)$$

This corresponds to a uniform perpendicular magnetic field B in the area containing the ring, the two point contacts, and the widening region connecting the point contacts to the external leads (see gray rectangle in Fig. 1, top part). For technical reasons, the magnetic field is set to zero in the external leads. We calculate the transmission matrix numerically and then obtain the conductance from the Landauer formula [2].

3. Results and discussion

3.1. Preliminary: a zero-field conductance

To analyze the operation of the valley filters attached to a ring with an irregular boundary, we first show in Fig. 2 the conductance in zero magnetic field. We take $\mu = 0.05\tau$ to keep $n = 1$ at the first constriction (the polarizer), and vary the Fermi energy μ' at the second constriction (the analyzer). For positive μ' ($n' = 1$), when the two constrictions transmit the same valley polarization, the narrowest rings show a strong conductance suppression, with $G \lesssim 10^{-5} e^2/h$ for $N = 1$, and $G \lesssim 10^{-2} e^2/h$ for $N = 3$. For negative μ' ($n' = -1$) the conductance additionally drops by two orders of magnitude, showing that the *valve effect* of Ref. [7] extends to the situation when transport is fully carried by evanescent modes. In wider rings ($N = 5$ and 7) we observe an appreciable current through the system. The conductance for $N = 5$ is still one order of magnitude below the optimal value $2e^2/h$, and the valve effect remains visible. For $N = 7$ the conductance spectrum is dominated by discrete resonance states, and the valve effect vanishes. (Let us notice that the resonances for $\mu' \lesssim -3\Delta/2$ are present in all spectra due to quasi-bound states [8] in the valence band of the second constriction.)

The anomalously small conductance for $N = 1$ can be attributed to mismatched valley polarization in subsequent sections of the ring arm, whose crystallographic orientation is close to zigzag lines rotated by $\pi/3$ [9]. It is also consistent with recent theoretical findings on the generic boundary condition of a terminated honeycomb lattice by Akhmerov and Beenakker [10]. It is shown that the zigzag boundary condition applies for any angle $\phi \neq 0 \pmod{\pi/3}$ of the boundary (where $\phi = 0$ labels the armchair orientation). The strong current suppression for $N = 3$, however, cannot be explained by existing numerical and analytical studies of ballistic systems. (Let us notice that we intentionally leave some dangling bonds on our ring edges to go beyond the theory of Ref. [10] limited to minimal edges.) Instead, it is consistent with experimental work of Ref. [5], showing even the mesoscopic ring of 0.7 μm diameter (in comparison with $2R = 70\sqrt{3}a \approx 30$nm in this study) needs to

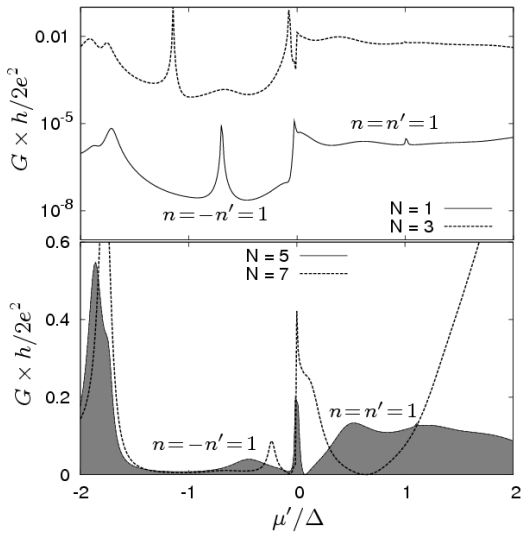

Fig. 2. Conductance of the graphene ring of Fig. 1 in zero magnetic field at fixed $\mu = 0.05\tau \approx \Delta/3$ as a function of μ'/Δ. The parameter $\mu' = \mu_\infty - U'$ is varied by varying U' at fixed μ_∞. (top) The data for $N = 1$ (solid line) and 3 (dashed line) on a logarithmic scale. (bottom) The data for $N = 5$ (solid line with shadowed area) and 7 (dashed line).

be heavily doped to open transmission channels and, in turn, show an appreciable conductance.

3.2. Magnetoconductance analysis

In Fig. 3 the conductance G is plotted as a function of the flux $\Phi = B\bar{S}$ through the ring, where $\bar{S} = (S_\mathrm{o} + S_\mathrm{i})/2$ is the average of the outer and inner ring areas S_o and S_i. The first harmonic frequency of the Fourier spectrum shown in Fig. 4 is within a few percent of the expected value $\Phi_0^{-1} = e/h$, indicating that $\bar{S}$ accurately represents the effective area of the ring. The harmonic content of the magnetoconductance oscillations is strikingly different when the current is strongly suppressed ($N = 1$ and 3, top two parts in Fig. 3) and when it is not suppressed ($N = 5, 7$, lower two parts). On the one hand, when the conductance is suppressed below $10^{-2}e^2/h$ the magnetoconductance oscillations are nearly sinusoidal, almost without higher harmonics. This is as expected for transmission through evanescent modes. On the other hand, when the conductance is of order e^2/h the oscillations are highly nonsinusoidal, with appreciable higher harmonics, as expected for transmission through propagating modes.

An interesting feature of the nonsinusoidal magnetoconductance oscillations shown in Fig. 3, and quantified by the Fourier transform in Fig. 4, is the suppression of the lowest harmonic (period $\Delta\Phi = \Phi_0$) in the case of opposite valley polarizations in the two constrictions ($n = -n' = 1$). This suppression of the fundamental periodicity is visible for an intermediate ring width $W = 15\sqrt{3}a$ corresponding to $N = 5$ (third part from top in Fig. 3 and top in Fig. 4), and vanishes for $N = 7$

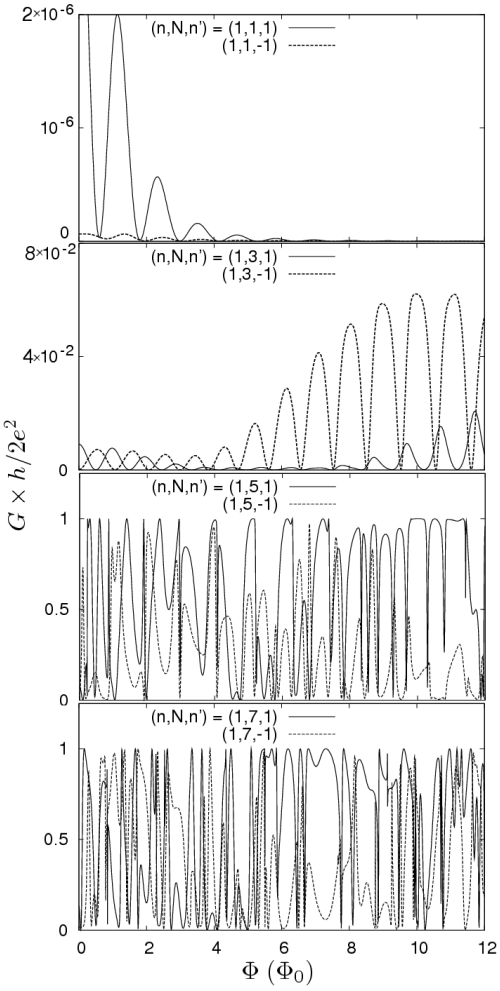

Fig. 3. Conductance as a function of magnetic flux through the ring. Solid curves show the case $n = n' = 1$, $\mu = \mu' = 0.05\tau$ of identical valley polarizations in both constrictions, and dashed curves show the case $n = -n' = 1$, $\mu = -\mu' = 0.05\tau$ of opposite polarizations. The value of N is varied between the four parts.

(fourth part from top and bottom part, respectively). The second (and higher) harmonics, in contrast, are unaffected in the case of opposite valley polarizations. The suppression of the first harmonic indicates that electrons which travel only once along the ring have a small probability for intervalley scattering and therefore cannot contribute to the conductance when the two constrictions have opposite valley polarization. Higher harmonics correspond to electrons which travel several times along the ring, with a larger probability for intervalley scattering and therefore a larger probability to contribute to the conductance. In other words, for the ring of intermediate width, typical intervalley scattering time is $t_\mathrm{valley} \gtrsim t_\mathrm{dwell}$ (with the semiclassical dwell time $t_\mathrm{dwell} \sim RW/(v_\mathrm{F}w)$) whereas for the widest ring $t_\mathrm{valley} \lesssim t_\mathrm{dwell}$. That suggests (i) t_valley weakly depends on W when R is kept constant, and (ii) it is relatively long, so the valley pseu-

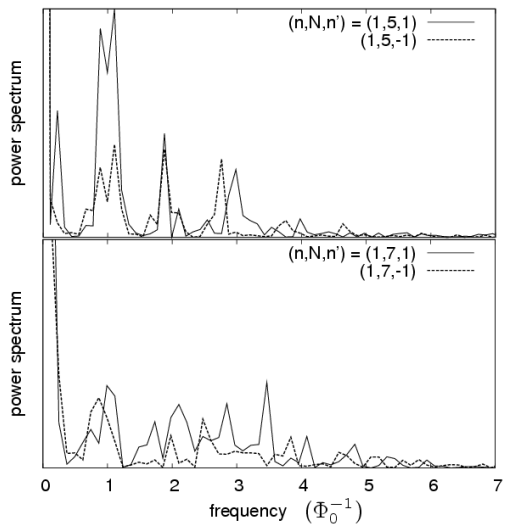

Fig. 4. Fourier transform of the magnetoconductance data shown in Fig. 3 for $N = 5$ and 7.

dospin is flipped rather after few than just one incidence with irregular ring edges.

4. Conclusions

In conclusion, we have identified signatures of valley polarization in the magnetoconductance of an Aharonov–Bohm interferometer in graphene. *First,* narrow rings show nearly sinusoidal magnetoconductance oscillations around a greatly suppressed average conductance, attributed to a generic current suppression effect in a constriction consists of two (or more) sections with crystallographic orientation rotated by an angle close to $\pi/3$. *Second*, the ring of an intermediate width shows suppression of the lowest harmonic of the conductance oscillations that appears when the two point contacts have opposite valley polarity, which indicates that electrons which have travelled only once along the ring preserve their valley polarization, and therefore cannot contribute to the conductance. The effect vanishes in a wide multimode ring, for which the Fourier spectrum of magnetoconductance oscillations shows that all harmonics are almost equally represented, and insensitive to valley polarity of the point contacts attached to the ring.

Acknowledgments

This work was supported by a special grant of the Polish Science Foundation (FNP), the Polish Ministry of Science (grant No. 1-P03B-001-29), and partly by the Alexander von Humboldt Stiftung-Foundation. Discussions with Anton Akhmerov and Patrik Recher are gratefully acknowledged. Special thanks are addressed to Prof. C.W.J. Beenakker for numerous discussions and correspondence.

References

[1] A.K. Geim, K.S. Novoselov, *Nature Mat.* **6**, 183 (2007).

[2] Y. Imry, *Introduction to Mesoscopic Physics*, Oxford University, Oxford 1996.

[3] Y. Aharonov, D. Bohm, *Phys. Rev.* **115**, 485 (1959).

[4] Y. Imry, R.A. Webb, *Sci. Am.* **260**, 36 (1989).

[5] S. Russo, J.B. Oostinga, D. Wehenkel, H.B. Heersche, S.S. Sobhani, L.M.K. Vandersypen, A.F. Morpurgo, *Phys. Rev. B* **77**, 085413 (2008).

[6] P. Recher, B. Trauzettel A. Rycerz, Ya.M. Blanter, C.W.J. Beenakker, A.F. Morpurgo, *Phys. Rev. B* **76**, 235404 (2007).

[7] A. Rycerz, J. Tworzydło, C.W.J. Beenakker, *Nature Phys.* **3**, 172 (2007).

[8] P.G. Silvestrov, K.B. Efetov, *Phys. Rev. Lett.* **98**, 016802 (2007).

[9] A. Rycerz, *Phys. Stat. Sol. A* **205**, 1281 (2008).

[10] A.R. Akhmerov, C.W.J. Beenakker, *Phys. Rev. B* **77**, 085423 (2008).